JAAS

PAPER

View Article Online
View Journal | View Issue

Cite this: *J. Anal. At. Spectrom.*, 2021, **36**, 786

Nano-bismuth sulfide based dispersive micro-solid phase extraction combined with energy dispersive X-ray fluorescence spectrometry for determination of mercury ions in waters

Katarzyna Pytlakowska, *[a] Ewa Malicka,[a] Ewa Talik[b] and Anna Gągor[c]

A selective method for the determination of mercury ions in different types of water samples by energy dispersive X-ray fluorescence spectrometry (EDXRF) was developed. Quantification of Hg(II) by EDXRF was preceded by ultra-sound assisted dispersive micro-solid phase extraction (USA-DMSPE) on nano-bismuth sulfide (nano-Bi_2S_3) as a solid sorbent. At pH 1 nano-Bi_2S_3 selectively adsorbs Hg(II) ions from aqueous samples with an adsorption capacity of 499.1 mg g^{-1}. The experimental data fitted well with the Langmuir isotherm model, which confirms the chemical character of the adsorption process. Under optimized preconcentration conditions, *i.e.* a sample pH of 1, adsorbent mass of 1 mg, sample volume of 50 mL and sonication time of 15 min, the linear response between fluorescence radiation intensity and the metal concentration was obtained within 1–200 ng mL^{-1} range with a correlation coefficient of 0.9988. The method allows the detection of mercury ions at a concentration of only 0.06 ng mL^{-1}. The determination of Hg(II) ions after the nano-Bi_2S_3 based USA-DMSPE-EDXRF procedure is possible even in the presence of a high concentration of anions and cations typically coexisting in surface waters. The described method was applied to the determination of Hg(II) ions in mineral, spring, river, and artificial sea waters. The correctness of the procedure was confirmed by analysis of the certified reference material (Seawater QC3163).

Received 19th November 2020
Accepted 4th February 2021

DOI: 10.1039/d0ja00477d

rsc.li/jaas

Introduction

Contamination of water by mercury is of particular concern due to the high toxicity of its compounds. According to the World Health Organization (WHO) directive mercury is classified into the first group of the most hazardous substances.[1] There are two main sources of mercury in aquatic systems, namely natural earth processes (*i.e.* volcanic and geothermal activity, soil and rock erosion, and biomass and forest burning) and anthropogenic ones. Mercury is introduced into waters mainly as a result of its widespread usage in agriculture as a fungicide and herbicide, fossil fuel combustion, metal and cement production, chlor-alkali industry activities, use of medical waste incinerators, or municipal waste combustion.[2] Mercury occurs in surface water mainly as soluble inorganic Hg(II). Depending on water pH and the chloride concentration it can form hydroxide and chloride ions. Some of Hg(II) may react with organic matter present in the aquatic ecosystem or transform into organic species as a result of microorganism activity.[3,4] Both organic and inorganic compounds are detrimental to the environment. They destroy natural aquatic ecosystems and, if they are introduced into the food chain, can cause serious disruption including kidney and neurological disorders in humans. Thus, constant monitoring of Hg(II) ions in water is important. The permissible mercury level in drinking water, recommended by the WHO is 0.001 mg L^{-1}, while the Environmental Protection Agency (EPA) allows the content of no more than 0.002 mg L^{-1}.[5,6] Since mercury occurs in the aquatic environment at an ultra-trace level, highly sensitive techniques are mandatory for its determination. For this purpose, cold vapor atomic absorption spectrometry (CVAAS),[7] cold vapor atomic fluorescence spectrometry (AFS),[8] inductively coupled plasma optical emission spectrometry (ICP-OES)[9] and inductively coupled plasma mass spectrometry (ICP-MS)[10,11] are the most commonly used ones. Despite their high sensitivity and wide dynamic range, problems associated with matrix and the memory effects caused by the contamination of the instruments, *i.e.* the sample introduction system, spray chamber and nebulizer, make the direct determination of mercury in environmental samples difficult.[12] Thus, the preconcentration step following measurements is usually needed.

X-ray fluorescence spectrometry (XRF), namely energy dispersive X-ray fluorescence spectrometry (EDXRF),[13,14]

[a]*Institute of Chemistry, University of Silesia, Szkolna 9, 40-006 Katowice, Poland. E-mail: katarzyna.pytlakowska@us.edu.pl*

[b]*Institute of Physics, University of Silesia, 75 Pułku Piechoty 1a, 41-500 Chorzów, Poland*

[c]*Faculty of Materials Science and Ceramics, University of Science and Technology, al. Mickiewicza 30, 30-059 Krakow, Poland*

wavelength dispersive X-ray fluorescence spectrometry (WDXRF)[15] and total reflection X-ray fluorescence spectrometry (TXRF),[16] has also been proposed for mercury determination. Although XRF enables the direct determination of metal ions in solid and liquid samples without or with minimal sample handling, it is rarely used for direct liquid analysis. This is due to several limitations including poor sensitivity (determination at the mg L^{-1} level), a narrow linear range, or matrix effects imposing the requirement for rigorous standards with matrices similar to those of the examined samples.[15] Moreover, evaporation of liquids during measurements and formation of bubbles may also disturb correct determination of analytes. In order to improve detection limits the preconcentration step is usually required in XRF analyses. Considering that XRF works best on solid samples, the most commonly used pretreatment technique prior to XRF measurements is solid phase extraction (SPE). Since the introduction of solid phase microextraction (SPME) and nanoadsorbents, the number of methods developed for the determination of analytes in liquid samples by the XRF technique has significantly increased. The use of nanoadsorbents in the SPME process is particularly profitable in combination with XRF due to the fact that the particle size effects can be neglected because of the very small size of nanoparticles. Moreover, a single experiment can be performed with ≥1 mg of nanoadsorbent, which leads to solid samples in the form of a thin layer. Given that in such samples matrix effects are compensated and matrix correction (mainly absorption effects) is not necessary, quantitative EDXRF analysis can be easily performed.[17,18] Furthermore, compared to the approaches based on combination of SPME with AAS, ICP-OES or ICP-MS, adsorbed metal ions on nanomaterials are directly measured by XRF. It overcomes problems associated with incomplete elution of analytes, sample contamination and analyte loss. Minimized sample handling and reduction of the chemical amount are the additional benefits of the SPME-XRF mode.

Among numerous nano-sized materials metal sulfide nanoparticles, including bismuth trisulfide (nano-Bi_2S_3), applied as nano-semiconductors have been widely explored in recent years. They have found applications in various branches of technology, *e.g.* photovoltaics, optoelectronic, thermoelectric, and solar cell devices, H_2 sensing or X-ray computed tomography imaging.[19] Nano-Bi_2S_3 has received special attention from the standpoint of environmental applications due to its non-toxicity, low cost and thermo-chemical stability.[20] A large number of donor S atoms that act as a soft base enable formation of strong bonds with soft and relatively soft metals making nano-Bi_2S_3 a selective adsorbent. On the other hand its weak interaction with alkali and alkaline earth cations that behave as hard acids allows it to be used in samples with high salinity without affecting their adsorption properties. Taking all these facts into account, nano-Bi_2S_3 seems to be a promising adsorbent and could find application in the water purification process.

The aim of this study was to develop a selective method for energy dispersive X-ray fluorescence spectrometric determination of mercury ions in different types of water samples including high salinity ones. EDXRF quantification was preceded by ultra-sound assisted dispersive micro-solid phase extraction (USA-DMSPE) on nano-Bi_2S_3 as a solid adsorbent. Nano-Bi_2S_3 was synthesized by a hydrothermal method. Its structure was confirmed by powder X-ray diffraction (XRD), EDXRF, and scanning electron microscopy (SEM). In order to optimize the USA-DMSPE performance, the influence of parameters such as sample pH, the adsorption time *vs.* sample volume, and the contact time were carefully studied. The method was applied for the determination of Hg(II) ions in mineral, spring, river, and artificial sea waters. The accuracy of the procedure was confirmed by analyzing the certified material (Seawater QC3163).

Experimental

Chemicals and reagents

All experiments were performed using water from a Milli-Q system (Millipore, Molsheim, France). Stock solutions (1 mg mL^{-1} of Hg(II), V(V), As(III), As(V), Se(IV), Se(VI), Cr(III), Cr(VI), Co(II), Ni(II), Cu(II), Zn(II), and Pb(II)), ammonium hydroxide solution (25%, Suprapur®) and nitric acid (65%, Suprapur®) were purchased from Merck (Darmstadt, Germany). Hydrochloride acid, ethanol and salts used for the studies of the influence of coexisting ions, were purchased from POCH (Gliwice, Poland). L-Cysteine and bismuth chloride, and certified material Seawater QC3163 were purchased from Sigma-Aldrich (Laramie, Wyoming, USA).

Instrumentation

Both determination of mercury(II) and adsorption studies were performed with an energy dispersive X-ray fluorescence spectrometer Epsilon 3 (PANalytical, Almelo, The Netherlands). The spectrometer is equipped with a Rh target X-ray tube of maximum power 9 W and a thermoelectrically cooled silicon drift detector (SDD) with 8 μm Be window and a resolution of 135 eV at 5.9 keV. The focal size of the X-ray beam, calculated as the full width in the middle of the maximum, is approximately 5.9 mm. The measurements were conducted using the following operating parameters: X-ray tube – 30 kV and 0.300 mA, primary beam filter – 100 μm Ag, counting time – 300 s, and atmospheric conditions. For the spectrum evaluation the Epsilon 3 Software was used. The spectral estimation procedure was based on a non-linear least-squares fit based on the AXIL algorithm. To verify the concentration of Hg(II) during adsorption studies ICP-OES measurements were also carried out. The concentration of Hg(II) in filtrates obtained after the preconcentration step was measured on a Spectroblue spectrometer (Spectro Analytical Instruments GmbH, Germany) with the following settings: plasma power – 1.4 kW, coolant gas – Ar, 12 L min^{-1}, auxiliary gas – Ar, 1 L min^{-1}, nebulizer gas – Ar, 1 L min^{-1}, nebulizer pressure – 3.2 bar, nebulizer – cross-flow type, sample uptake rate – 2 mL min^{-1}, wavelength – 253.652 nm, 3 replicates, and integration time – 10 s.

The powder diffraction data were collected using an X'Pert PRO equipped with a PIXcel ultra-fast line detector and Soller

slits for Cu K_α radiation. The samples were measured in a reflection mode using the Bragg–Brentano geometry. Le Bail profile matching was performed with Jana2006.[21]

The nano-Bi_2S_3 surface images were collected using a JEOL-5410 SEM equipped with an energy dispersion X-ray spectrometer (EDS with Si(Li) X-ray detector). The pressure in the measuring chamber ranged from 10^{-4} to 10^{-5} Pa.

Other apparatuses used during experiments were as follows: a pH-meter (Mettler, Toledo) equipped with a combined glass electrode, a Teflon-lined stainless steel autoclave, a centrifuge (MPW Med. Instruments, model MPW-350), an ultrasonic bath (Bandelin Sonorex), a microanalytical balance (Radwag, model MYA 2.3Y), a magnetic stirrer (Thermo Scientific, Cimarec), and a set for filtration under reduced pressure (Millipore) equipped with a filtration assembly of 5 mm and 20 mm diameters.

Synthesis of nano-Bi_2S_3

Nano-Bi_2S_3 was synthesized by the biomolecule-assisted hydrothermal method reported by Zhang and Chen with some modifications.[22] Briefly, 2 mmol of $BiCl_3$ was dissolved in 40 mL of water and after adjusting sample pH to 6.5, 4 mmol of L-cysteine was added. The solution was mixed with a magnetic stirrer for 1 h to obtain a homogenous mixture. Next, the solution was transferred into a Teflon-lined stainless steel autoclave and heated at 180 °C for 12 h in a laboratory dryer. The resulting black precipitate was separated by centrifugation, washed several times with ethanol and water, and dried at 80 °C.

Batch adsorption experiments

25 mL-in volume samples containing Hg(II) ions at different concentrations and 1 mg of nano-Bi_2S_3 were stirred at 900 rpm for 3 hours at room temperature after pH adjustment to 1 with HCl. Then, the suspensions were filtered through membrane filters (0.22 μm) under reduced pressure. After drying, filters covered with nano-Bi_2S_3 and adsorbed Hg(II) ions were directly assessed by EDXRF. Knowing the initial concentration of Hg(II) in the aqueous sample (C_o, mg L^{-1}), and the concentration of the adsorbed Hg(II) ions on the nano-Bi_2S_3 surface (mg g^{-1}), the equilibrium concentration (C_e, mg L^{-1}) was computed using the following equation: $C_e = C_o - (q_e m/V)$, where V is the suspension volume, and m is the nano-Bi_2S_3 dosage (mg).

Preconcentration procedure

50 mL-in volume samples containing Hg(II) ions and 1 mg of nano-Bi_2S_3, after adjustment pH to 1 with HCl, were sonicated for 15 min. The suspensions were then filtered through an adapted 5 mm diameter filtration unit using Millipore nitrocellulose membrane filters of 0.22 μm pore size and 30 mm diameter. After drying at room temperature, the filters coated with the nanomaterial and adsorbed ions Hg(II) were assessed by EDXRF. To prepare the blank sample high-purity water was used and the procedure described above was performed.

Real samples and sample preparation

Samples of spring and river waters, collected in the Upper Silesian region, Poland, were filtered through a Millipore cellulose acetate membrane (0.22 μm), acidified with HNO_3 and stored at 4 °C before the analysis. Mineral water was purchased at the local market and used without any preparation step. Artificial seawater was obtained by dissolving 21.03 g NaCl, 3.52 g Na_2SO_4, 0.61 g KCl, 0.088 g KBr, 0.034 g $Na_2B_4O_7 \cdot 10H_2O$, 9.50 g $MgCl_2 \cdot 6H_2O$, 1.32 g $CaCl_2 \cdot 2H_2O$, 0.02 g $SrCl_2 \cdot 6H_2O$ and 0.02 g $NaHCO_3$ in 1 L of water.[23]

Results and discussion

Characterization of nano-Bi_2S_3

Nano-Bi_2S_3 synthesized by the hydrothermal method was characterized by XRD, EDXRF and SEM techniques. In Fig. 1 the XRD pattern, and the Le Bail fit of the Bi_2S_3 nano-powder, and annealed Bi_2S_3 are presented. All diffraction peaks are attributed to the orthorhombic *Pnma* phase of Bi_2S_3. The final compliance of R factors for the profile (GOF = 1.30, R_p = 1.25, wR_p = 1.63), and the obtained lattice parameters (a = 11.320, b = 3.989, c = 11.115) with the JCPDS card No. 17-0320,[24] proves the formation of an orthorhombic crystal system. The sample annealing, presented in Fig. 1b, confirms the growth of the crystallites. The mean size of the synthesized crystallites calculated from the Scherrer formula is 112 ± 2 nm. The XRD pattern of the annealed sample is characteristic of nano-powders. Additionally, the XRD patterns together with EDS analysis (57.14 atomic% of S and 42.86 atomic% of Bi) confirm the high purity of the synthesized Bi_2S_3.

In Fig. 2a the EDXRF spectrum of the nano-Bi_2S_3 is presented. The peaks at 9.42 keV, 10.84 keV, 13.02 keV, and 15.25 keV are assigned to Bi L_l, Bi Lα1, Bi Lβ1, and Bi Lγ1, respectively. The peak at 2.4 keV consists of four overlapped peaks, namely S Kα at 2.31 keV, S Kβ at 2.46 keV, and Bi Mα1 and Bi Mα2 at 2.42 keV.

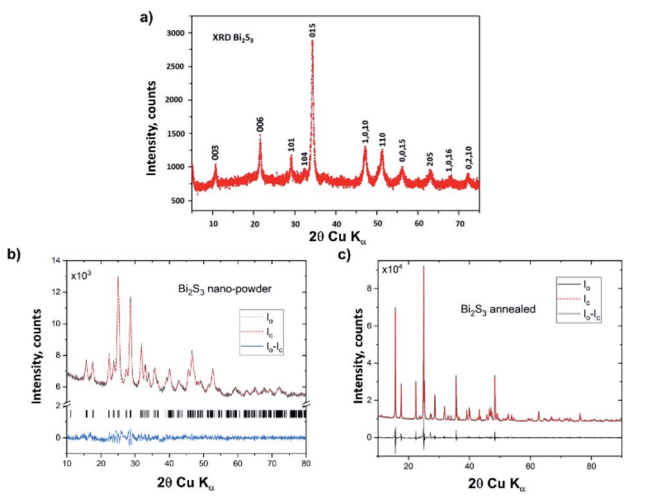

Fig. 1 (a) The XRD pattern of Bi_2S_3, (b) the Le Bail fit of the Bi_2S_3 nano-powder and (c) the Le Bail fit of annealed Bi_2S_3. I_o and I_c denote the observed and calculated intensities, respectively.

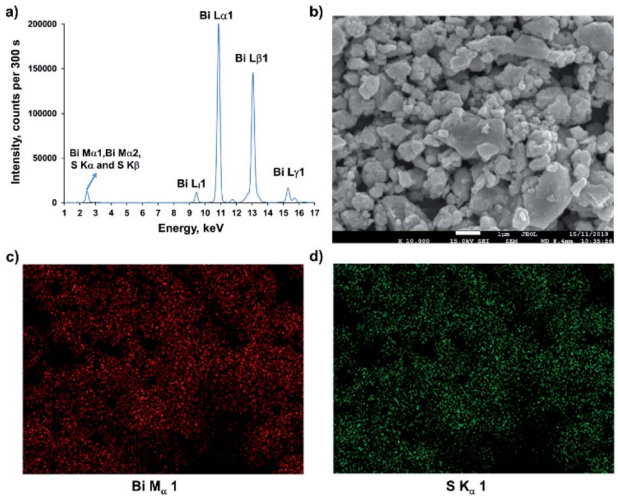

Fig. 2 (a) EDXRF spectrum of nano-Bi_2S_3, (b) SEM image of nano-Bi_2S_3, and (c and d) SEM/EDS images of the synthesized nano-Bi_2S_3 surface with the distribution of Bi and S elements on the nano-Bi_2S_3 surface.

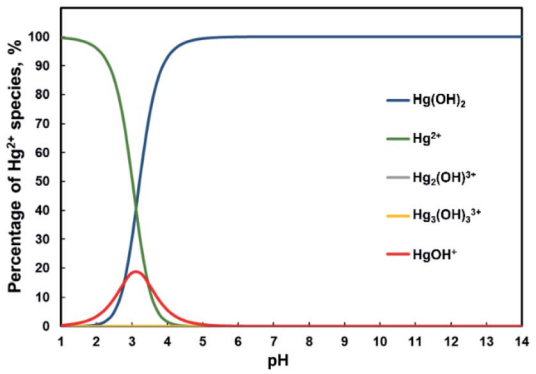

Fig. 3 Speciation distribution diagram for Hg(II) species depending on sample pH.[27]

The SEM/EDS images of nano-Bi_2S_3, depicting its shape and the correlation between the distribution of Bi and S elements on the nano-Bi_2S_3 surface are shown in Fig. 2b–d respectively. The nanomaterial synthesized by the hydrothermal method in nearly neutral solution consists mainly of irregular particles ranging in sizes from the sub-micrometer to micrometer scale. Such a morphology is in accordance with the products synthesized by Lu *et al.*[25] and Phuruangrat *et al.*,[26] and proves strong influence of synthesis conditions on the product morphology by controlling the nucleation and growth processes.

Effect of sample pH

Sample pH has a significant impact on the adsorption process. It affects both the speciation distribution of analyte species in aqueous samples and the protonation/deprotonation of the adsorbent functional groups. Moreover, the charge distribution on the adsorbent surface can be substantial from the standpoint of the adsorption mechanism. It should be noted here that the capture of analyte ions on the adsorbent surface may result from electrostatic interactions, ion exchange or complexation reactions. However, in most cases, all of these processes occur at the same time.

The speciation distribution diagram of Hg(II) species at different sample pH values calculated using the MINTEQA2 program[27] presented in Fig. 3, shows that mercury may occur in the aqueous medium as Hg^{2+}, $HgOH^+$, $Hg_2(OH)^{3+}$, $Hg_3(OH)_3^{3+}$ and $Hg(OH)_2$. Under acidic conditions Hg^{2+} ions dominate while in solutions of pH higher than 5 mercury precipitates as $Hg(OH)_2$ which may disturb the adsorption process. Thus, it was anticipated that in acidic media electrostatic interactions would play a minor role in the adsorption mechanism due to the repulsion between the positively charged nano-Bi_2S_3 surface and cationic mercury species. But taking into account the theory of soft and hard acids and bases (HSAB) it was expected that in the adsorption process the complexation reaction would be involved. According to HSAB theory sulfur is classified as a soft base and Hg(II) ions are considered to be a soft acid. Thus, the interaction between Hg(II) and S atoms should be strong. In order to select the optimal pH conditions for the adsorption of mercury ions, a sample batch of the same volume containing a constant amount of adsorbent, the same concentration of examined ions, and sonication for the same time was prepared. The affinity of nano-Bi_2S_3 towards Hg(II), V(V), Cr(III), Cr(VI), As(III), As(V), Se(IV), Se(VI), Co(II), Ni(II), Cu(II), Zn(II) and Pb(II) species was investigated within the pH range 1–10.

As can be seen in Fig. 4a in acidic media adsorption of Hg(II) ions on the nano-Bi_2S_3 surface is selective. The highest extraction efficiency of *ca.* 80% is reached at pH 1 (in HNO_3 media). A further increase of sample pH results in the decrease of adsorption up to pH 5. At neutral and basic pH the increase in the adsorption percentage is partially due to the precipitation of $Hg(OH)_2$. The remaining studied anions, namely V(V), Cr(VI), As(III), As(V), Se(IV), and Se(VI) are not quantitatively adsorbed on nano-Bi_2S_3 over the studied pH range. In the case of Cr(III), Co(II), Ni(II), Cu(II), Zn(II) and Pb(II) cations adsorption increase with the sample pH reaching the highest values in basic media.

Considering that the adsorption of Hg(II) ions on the nano-Bi_2S_3 surface occurs in acidic media, the influence of nitric acid and hydrochloric acid on the extraction efficiency was examined. If the adsorption process is carried out in a nitric acid environment, then from the standpoint of HSAB theory the adsorption of mercury ions results from the complexation reaction. When HCl is used to acidify the sample solution, Hg(II) can form negatively charged chloride complexes. Given that the surface of the nanoadsorbent is protonated at pH 1, an electrostatic interaction between the positively charged adsorbent and the negatively charged mercury chloride complexes is also possible. As a result of the additional interaction an increase in adsorption efficiency up to 99% is observed. Therefore, HCl was used to adjust the sample pH in the course of further studies.

Effect of the adsorption time and sample volume

Extraction efficiency is also affected by the sample volume and contact time between analyte ions and the adsorbent. Typically,

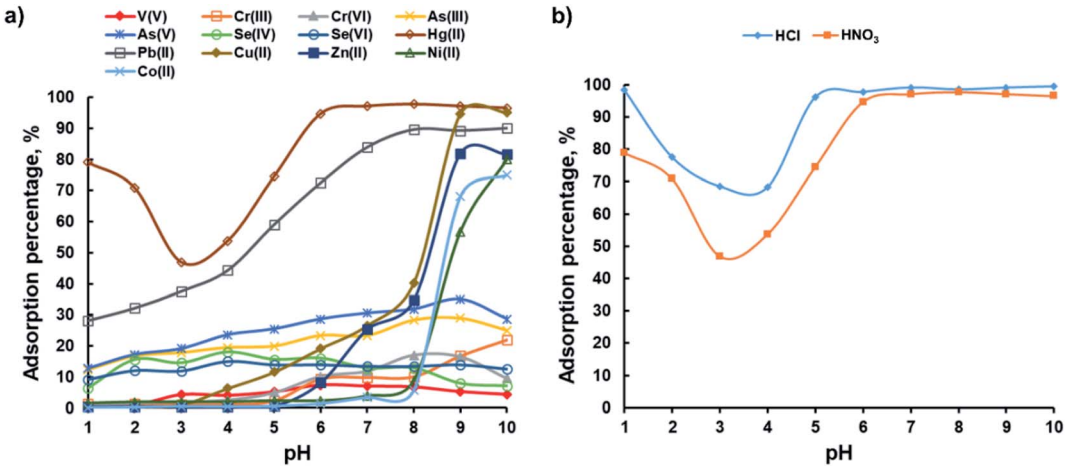

Fig. 4 (a) The influence of pH (sample volume 50 mL, metal ion concentration 100 ng mL^{-1}, adsorbent mass 1 mg, sonication time 15 min, $n = 3$) on the recovery of (a) Hg(II), V(V), Cr(III), Cr(VI), As(III), As(V), Se(IV), Se(VI), Co(II), Ni(II), Cu(II), Zn(II) and Pb(II) species by the USA-DMSPE-EDXRF procedure, (b) the influence of acid type used for sample pH adjustment (sample volume 50 mL, Hg(II) concentration 100 ng mL^{-1}, pH 1, adsorbent dosage 1 mg, sonication time 15 min, $n = 3$) on Hg(II) recovery by the USA-DMSPE-EDXRF procedure.

the mass transfer rate decreases with the increase of sample volume. As a result the time required to complete the adsorption process as well as the filtration step increases. In order to find a compromise between the sample volume and adsorption time, both the parameters were examined simultaneously. Additionally, ultrasound and mixing were used to accelerate the extraction process. Optimization of the contact time and sample volume was performed in the range of 0–100 min and 25–75 mL, respectively.

As shown in Fig. 5, the time required to complete the adsorption process is almost 5 times shorter with ultrasound assistance than with mechanical agitation. In the case of samples with a volume of 25 mL, the highest adsorption of Hg(II) ions on the nano-Bi_2S_3 surface was obtained after 10 and 40 minutes by means of ultrasonication and stirring, respectively. For the samples of 75 mL the contact time assuring quantitative adsorption was prolonged to 25 and 70 minutes. Taking into account the optimized parameters together with the filtration time, in the course of further studies, ultrasound-assisted extraction of Hg(II) ions was selected for samples with a volume of 50 mL, for which the contact time of the analyte with the adsorbent surface was 15 minutes.

Adsorption capacity of GO-S

The Langmuir[28] and Freundlich[29] isotherm models were used to explain the Hg(II) ion adsorption mechanism on the nano-Bi_2S_3 surface. The following equations were used to calculate the isotherms:

$$q_e = \frac{q_{max} K_L C_e}{1 + K_L C_e} \quad \text{and} \quad q_e = K_F C_e^{1/n}$$

where q_e is the amount of metal adsorbed per unit of the adsorbent mass at equilibrium (mg g^{-1}), q_{max} is the maximum amount of Hg(II) ions adsorbed on 1 mg of the nano-Bi_2S_3 surface with a monolayer coverage at the highest equilibrium ion concentration (mg g^{-1}), K_L is the adsorption enthalpy (L mg^{-1}), and K_F (mg^{1-n} L^n g^{-1}) and n are Freundlich constants related to the adsorption ability and adsorption intensity, respectively.

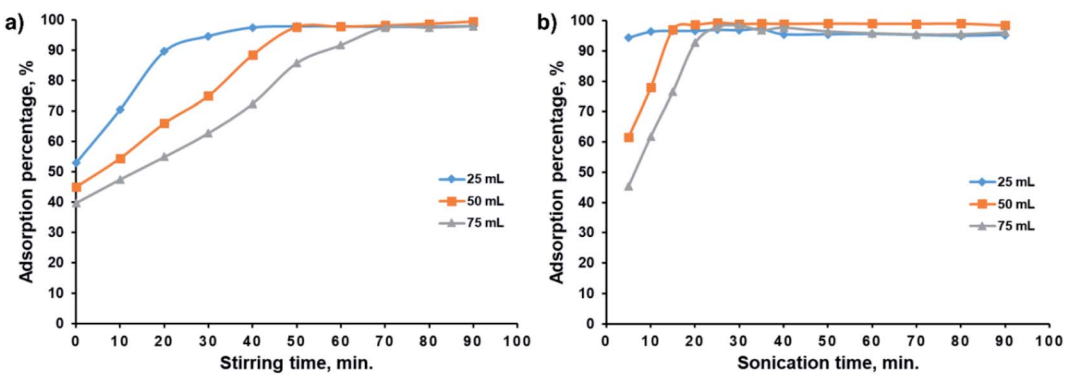

Fig. 5 Influence of the (a) stirring time or the (b) sonication time and sample volume on extraction efficiency, given as the recovery percentage, of Hg(II) ions (sample pH = 1, adsorbent dosage 1 mg, Hg(II) ion concentration 100 ng mL^{-1}).

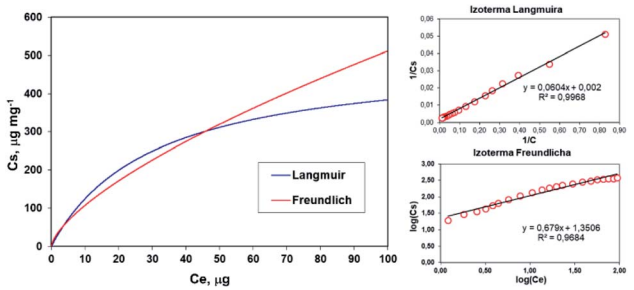

Fig. 6 The Langmuir and Freundlich adsorption isotherms for Hg(II) ions (sample pH = 1, adsorbent mass 1 mg, $T = 20$ °C, contact time 180 min).

Fig. 6 shows the patterns of adsorption isotherms along with the parameters obtained by fitting the experimental data to the Langmuir and Freundlich isotherm models. As can be seen, the experimental data are described better by the Langmuir isotherm model than the Freundlich model, which suggests the chemisorptive nature of the process, observed in the formation of coordination bonds between Hg(II) ions and S atoms present on the Bi_2S_3 nano-surface. Furthermore, the n value computed from the Freundlich isotherm indicates the dominant role of adsorption in the examined system.[30] Table 1 shows the comparison of the adsorption capacity of recently reported sulfur-containing nanoadsorbents used for mercury removal. The presented data show the excellent adsorption properties of nano-Bi_2S_3 towards Hg(II) ions compared to other nanomaterials.

Analytical characteristics

An exemplary EDXRF spectrum recorded for the optimal preconcentration conditions of Hg(II) ions on nano-Bi_2S_3 is shown in Fig. 7.

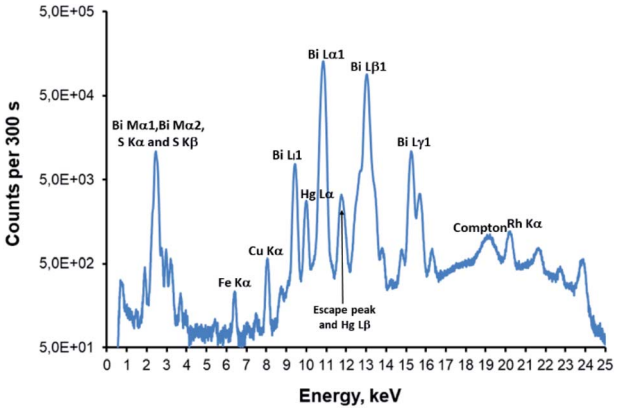

Fig. 7 EDXRF spectrum recorded for the optimal preconcentration conditions of Hg(II) ions on nano-Bi_2S_3 (measurement conditions: 30 kV and 0.300 mA, primary beam filter – 100 μm Ag, counting time – 300 s, Hg(II) concentration – 60 ng mL^{-1}; the vertical scale is logarithmic).

In the resulting EDXRF spectrum, peaks from Hg Lα (9.99 keV) and Bi L_l, Bi Lα1, Bi Lβ1, and Bi Lγ1 (9.42 keV, 10.84 keV, 13.02 keV, and 15.25 keV) are identified. The Hg Lβ peak is overlapped by the escape peak from Bi Lβ1. The peak at 2.4 keV consists of four overlapped peaks, namely S Kα at 2.31 keV, S Kβ at 2.46 keV, and Bi Mα1 and Bi Mα2 at 2.42 keV. Additional peaks from Cu and Fe probably come from the instrument components itself. It can also be observed that Rh and Compton peaks are of low intensity due to the thin layer method. The net intensities of Hg Lα were calculated using a non-linear least-squares fit based on the AXIL algorithm (Epsilon 3 Software).

For the analytical characterization of the USA-DMSPE-EDXRF method for divalent mercury determination some parameters, *i.e.* the linearity range, detection and quantification limits, precision at two concentrations of Hg(II) ions and recovery were determined. The calibration curve in the range 1

Table 1 Comparison of the adsorption capacity of sulfur-containing nanoadsorbents with respect to Hg(II) ions[a]

Adsorbent	pH	q_{max}, mg g^{-1}	Ref.
CNT/Fe_3O_4-TSC	6	172.83	31
MoS_2	6	160.4	32
rGO-PDTC/Fe_3O_4	6	181.82	33
GO-TSC	3.5	231	34
LGO/S-doped g-C_3N_4 nanotube	5	141	35
GO/MBT	5.4–6.9	107.52	36
SGO/Fe–Mn	7	233.17	37
Nano-Bi_2S_3	1	499.1	This work

[a] CNT/Fe_3O_4-TSC – magnetite multiwalled carbon nanotubes functionalized by thiosemicarbazide; MoS_2 – molybdenum disulfide; rGO-PDTC/Fe_3O_4 – dithiocarbamate (DTC)-modified magnetic reduced graphene oxide; GO-TSC – thiosemicarbazide-grafted graphene oxide; LGO/S-doped g-C_3N_4 nanotube – framework based on large flake sized graphene oxide (LGO) combined with S-doped g-C_3N_4 nanotubes; GO/MBT – mercaptobenzothiazole (MBT) functionalized graphene oxide (GO); SGO/Fe–Mn – thiol-functionalized graphene oxide/Fe–Mn composite.

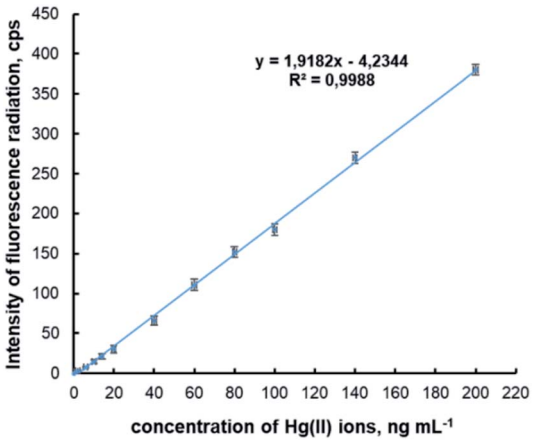

Fig. 8 Intensity of fluorescence radiation as a function of Hg(II) concentration (measurement conditions: 30 kV and 0.300 mA, primary beam filter – 100 μm Ag, counting time – 300 s). Error bars represent the standard deviation for $n = 3$.

to 200 ng mL^{-1} shows good linearity with the correlation coefficient of $R^2 = 0.9988$ (Fig. 8).

To calculate the detection and quantification limits the following formulas: LOD = $(3/k)(B/t)^{1/2}$ and LOQ = 3.3LOD, where k is the count sensitivity [s^{-1} μg^{-1}], B is the count rate of the blank sample [counts per s] and t is the counting time [s], were used. The computed values are found to be 0.06 and 0.198 ng mL^{-1}, respectively. It should be emphasized here that such low detection and quantification limits were obtained using a low-powered spectrometer of 9 W, with no cooling media and gas consumption. Taking into account the obtained LOD and LOQ as well as the EPA and WHO legislated limits of the Hg(II) concentration in drinking waters, the developed method is suitable for monitoring of the Hg(II) content in real water samples. To evaluate the precision of the method six replicates containing Hg(II) ions at concentrations of 5 and 20 ng mL^{-1} were measured. The relative standard deviations, expressed as RSD values of 4.8 and 2.7% demonstrate the satisfactory repeatability of the method. Recovery computed from the following equation: $R = (c_{USA\text{-}DMSPE}/c_{initial}) \times 100\%$, where R is the recovery, $c_{initial}$ is the concentration of Hg(II) ions introduced into the solution [$\mu g\ L^{-1}$], $c_{USA\text{-}DMSPE}$ is the concentration of Hg(II) determined after the preconcentration step [$\mu g\ L^{-1}$], within the linearity range changes from 96 to 102%.

The evaluated method was compared with the recently reported procedures devoted to the quantification of mercury(II),

Table 2 Comparison of the USA-DMSPE-EDXRF method for divalent mercury determination with the literature data (years 2016–2020)[a]

Adsorbent	Preconcentration technique	Technique	pH	Sample volume, mL	Adsorption time, min	LOD, $\mu g\ L^{-1}$	Linearity range, $\mu g\ L^{-1}$	Matrix	Ref.
Magnetic PAMAM dendrimers	MSPE	HPLC-VWD	8	100	60	0.040	0.1–200	Water	38
IL/MGO	MSPE	CV-AAS	4	25	8	0.57	1–200	Water, milk, omega-3 supplements and lipstick	39
MSCFM	Column SPE	ICP-OES	6	100	3	0.09	0.5–100	Water	40
mGO@SiO_2@2-MPATD	MSPE	CV-AAS	6.3	600	10	0.008	0.05–75	Water, seafood samples	41
MGO	MSPE	FI-ICP-OES	3	—	3	0.05	0.2–1000	Water	42
Fe_3O_4/g-C_3N_4	USA-MDMSPE	AFS	7	50	15	0.0037	0.01–0.6	Water	43
MWCNTs-Fe_3O_4 MNPs-silica-EET	MDMSPE	CV-AAS	6	10	2	1.5	9–1000	Water, hemodialysis solution and fish	44
Fe_3O_4@SiO_2-SH	MSPE	HPLC-ICP-MS	3–9	500	5	0.001	0.005–0.03	Water	45
TiO_2 NPs	USA DMSPE	CV-AAS	7.5	10	5 s	0.004	—	Water	46
PVC-based membrane functionalized with dithizone	SPE	TXRF	—	200	24 h	0.3	1–30	Water	13
PIM/TOMATS	SPE	EDXRF	7.2–8.3	500	24 h	0.2	0.6–10	Water	14
AAXAD-4	SPE	FI-CV-AAS	4	125		0.148	0.4–1.6	Water	47
MGO/thiophene	MDMSPE	FI-CV-AAS	6.5	50	21	0.025	1–85	Seafood	48
Nanomagnetic silica-based thiol-functionalized sorbent	MDSPE	CV-AAS	6	50	5	0.06	0.2–50	Human fluids	49
Nano-Bi_2S_3	DMSPE	EDXRF	1	50	15	0.06	1–200	Water	This work

[a] HPLC-VWD – high performance liquid-phase chromatography and ultraviolet variable wavelength detector (HPLC-VWD); FI-CV-AAS – flow injection cold vapor atomic absorption spectrometry; HPLC-ICP-MS – high performance liquid chromatography-inductively coupled plasma mass spectrometry; AFS – atomic fluorescence spectroscopy; CV-AAS – cold vapor atomic absorption spectrometry; ICP-OES – inductively coupled plasma optical emission spectrometry; EDXRF – energy dispersive X-ray fluorescence spectrometry; TXRF – total reflection X-ray fluorescence spectrometry; SPE – solid-phase extraction; MSPE – magnetic solid-phase extraction; USA DMSPE – ultrasound-assisted dispersive micro solid-phase extraction; MDMSPE – magnetic dispersive micro solid phase extraction; DMSPE – dispersive micro solid phase extraction; mGO@SiO_2@2-MPATD – 2-mercapto-5-phenylamino-1,3,4-thiadiazole (2-MPATD) modified magnetic graphene oxide coated with a silica layer; MGO – magnetic graphene oxide; AC – activated carbon; Fe_3O_4@SiO_2-SH – SiO_2 modified with thiol groups coated on the surface of Fe_3O_4 nanoparticles; PIM/TOMATS – polymer inclusion membrane (PIM) containing the task-specific ionic liquid trioctylmethylammonium thiosalicylate (TOMATS); AAXAD-4 – aminated Amberlite XAD-resin; MSCFM – cellulose nanofiber mats functionalized with MoS_2; Fe_3O_4 MNPs-silica-EET – nanomagnetite (Fe_3O_4)/chelating agent 1-(2-ethoxyphenyl)-3-(4-ethoxyphenyl)triazene functionalized multi-walled carbon nanotubes with a silica shell.

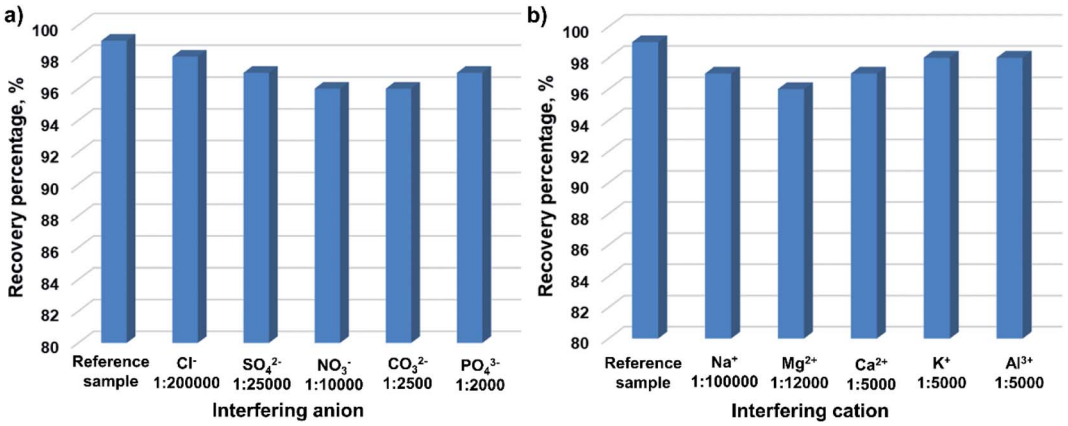

Fig. 9 Effect of typically coexisting ions (a) anions, (b) cations on the extraction efficiency of heavy metal ions (sample pH = 1, sample volume 50 mL, adsorbent dosage 1 mg, Hg(II) ion concentration 0.5 ng mL^{-1}, sonication time 15 min).

and the data are presented in Table 2. From the LOD point of view the developed procedure is not competitive with the most frequently applied approaches based on the combination of spectroscopic techniques, including AFS, and ICP-MS and in some cases CV-AAS, with the SPE step. But the main disadvantages of these methods are limited availability of equipment, difficulties in handling and high operating costs making their usage in routine analysis too expensive. Moreover, all of them operate on liquid samples and require an additional elution step that can be a source of errors resulting from analyte loss or sample contamination unlike the described EDXRF method.

Effect of coexisting ions

Coexisting anions (Cl^-, SO_4^{2-}, NO_3^-, CO_3^{2-}, HCO_3^-, and PO_4^{3-}) and cations (Na^+, K^+, Ca^{2+}, Mg^{2+}, and Al^{3+}) are important constituents in water samples, and may influence the adsorption of the target analyte as a result of competition to the same binding sites. Thus, a sample batch of the same volume containing a constant amount of adsorbent, the same concentration of 0.5 ng mL^{-1} of Hg(II) but various amounts of interfering species, and sonicated for the same time, was prepared. Variations in recovery ranging from $R \pm 5\%$ were accepted to establish a tolerable level of coexisting ions that does not affect the determination of Hg(II) by USA-DMSPE-EDXRF on nano-Bi_2S_3 as a solid adsorbent. As can be seen in Fig. 9 the naturally occurring cations and anions in water samples do not affect the adsorption of Hg(II) on the nano-Bi_2S_3 surface even at a high concentration. The resistance to high concentrations of cations can be explained by both the electrostatic repulsion between two positively charged specimens and the weak interaction between sulfur as a soft base and alkali and alkaline earth cations which act as hard acids. In the case of anions such phenomena may be due to weaker affinity for the positively charged nano-Bi_2S_3 surface than for Hg(II) ions. The obtained results show that the method may be applied to the determination of Hg(II) in water samples, even high salinity ones.

Table 3 Determination of Hg(II) ions in waters by the proposed method (uncertainties correspond to one standard deviation, $n = 3$, sample pH = 1, sample volume 50 mL, adsorbent dosage 1 mg, sonication time 15 min)

Sample	Added, ng mL^{-1}	Found, ng mL^{-1}	Recovery, %
Mineral water	0	<LOD	—
	5	4.85 ± 0.09	97
	20	19.7 ± 0.55	99
Spring water	0	<LOD	—
	5	4.91 ± 0.07	98
	20	19.6 ± 0.73	98
River water	0	<LOD	—
	5	4.78 ± 0.11	96
	20	19.5 ± 0.45	98
Artificial sea water	0	<LOD	—
	5	4.71 ± 0.08	94
	20	19.7 ± 0.84	99
Seawater QC3163	17.6 ± 0.314[a]	17.2 ± 0.6	98

[a] Certified value.

Application to water sample analysis

The utility of the USA-DMSPE-EDXRF procedure for the determination of mercury in waters was verified by analyzing real water samples and samples enriched with a known concentration of Hg(II) ions prepared according to the "Preconcentration procedure". In order to validate the method, the certified material Seawater QC3163 was analyzed. The results summarized in Table 3 confirm the usefulness of the method for the determination of Hg(II) ions in various types of water at trace and ultra-trace levels.

Conclusions

The procedure based on combination of ultra-sound assisted dispersive micro-solid phase extraction on nano-Bi_2S_3 with EDXRF determination of mercury(II) is described. Nano-Bi_2S_3 synthesized by a hydrothermal method exhibits excellent adsorption properties towards Hg(II) ions compared to other S-

based nanomaterials. The maximum adsorption capacity is 499.1 mg g^{-1}. Better adjustment of the data to the Langmuir isotherm model than the Freundlich model suggests the chemisorptive nature of the process, involving coordination binding between Hg(II) ions and S atoms. The method enables quantification of Hg(II) ions in aqueous samples at the μg L^{-1} level that is almost 1000-fold lower than the limit obtained in the direct analysis of water samples by EDXRF. Such a low detection limit was achieved with a low-power EDXRF spectrometer without any cooling media and gas consumption. The method exhibits high selectivity toward Hg(II) in acidic media and can be utilized for high salinity sample analyses. The main benefits of the developed procedure are simplicity, low operating cost, elimination of the elution step minimizing analyte loss or sample contamination, the wide linearity range, acceptable precision and accuracy confirmed by analysis of the Seawater QC3163 certified material. The proposed method can be performed in an easy manner without using any sophisticated equipment.

Conflicts of interest

There are no conflicts to declare.

References

1 *WHO recommended classification of pesticides by hazard and guidelines to classification 2019*, https://apps.who.int/iris/bitstream/handle/10665/332193/9789240005662-eng.pdf, accessed September 2020.
2 G. Liu, Y. Cai, N. O'Driscoll, X. Feng and G. Jiang, in *Environmental Chemistry and Toxicology of Mercury*, ed. G. Liu, Y. Cai and N. O'Driscoll, Wiley & Sons, New Jersey, 1st edn, 2012, vol. 1, pp. 1–12.
3 H. Hsu-Kim, K. H. Kucharzyk, T. Zhang and M. A. Deshusses, *Environ. Sci. Technol.*, 2013, **47**, 2441–2456.
4 F. M. M. Morel, A. M. L. Kraepiel and M. Amyot, *Annu. Rev. Ecol. Syst.*, 1998, **29**, 543–566.
5 *Council Directive 98/83/EC on the Quality of Water Intended for Human Consumption*, 1998, pp. 32–54.
6 United States Environmental Protection Agency, *National Primary Drinking Water Regulations*, https://www.epa.gov/ground-water-and-drinking-water/national-primary-drinking-water-regulations#Inorganic, accessed September 2020.
7 Z. Zhu, G. C. Y. Chan, S. J. Ray, X. Zhang and G. M. Hieftje, *Anal. Chem.*, 2008, **80**, 7043–7050.
8 P. R. Aranda, R. A. Gil, S. Moyano, I. De Vito and L. D. Martinez, *J. Hazard. Mater.*, 2009, **161**, 1399–1403.
9 X. Wu, W. Yang, M. Liu, X. Hou and C. Zheng, *J. Anal. At. Spectrom.*, 2011, **26**, 1204–1209.
10 X. Jia, Y. Han, C. Wei, T. Duan and H. Chen, *J. Anal. At. Spectrom.*, 2011, **26**, 1380–1386.
11 Y.-F. Li, C. Chen, B. Li, J. Sun, J. Wang, Y. Gao, Y. Zhao and Z. Chai, *J. Anal. At. Spectrom.*, 2006, **21**, 94–96.
12 X. Zhu and S. D. Alexandratos, *Microchem. J.*, 2007, **86**, 37–41.
13 V. S. Hatzistavros and N. G. Kallithrakas-Kontos, *Anal. Chim. Acta*, 2014, **809**, 25–29.
14 G. Elias, E. Marguí, S. Díez and C. Fontàs, *Anal. Chem.*, 2018, **90**, 4756–4763.
15 P. R. Aranda, L. Colombo, E. Perino, I. E. De Vito and J. Raba, *X-Ray Spectrom.*, 2013, **42**, 100–104.
16 E. Marguí, I. Queralt, M. Guerra and N. Kallithrakas-Kontos, *Spectrochim. Acta, Part B*, 2018, **149**, 84–90.
17 R. Sitko, *Spectrochim. Acta, Part B*, 2009, **64**, 1161–1172.
18 K. Pytlakowska, M. Pilch, B. Hachula, J. E. Nycz, K. Kornaus and W. A. Pisarski, *J. Anal. At. Spectrom.*, 2019, **34**, 1416–1425.
19 Y. Ramos Reynoso, A. Martinez-Ayala, M. Pal, F. Paraguay-Delgado and N. R. Mathews, *Adv. Powder Technol.*, 2018, **29**, 3561–3568.
20 Y. Xu, Z. Ren, G. Cao, W. Ren, K. Deng and Y. Zhong, *Phys. B*, 2010, **405**, 1353–1358.
21 V. Petricek, M. Dusek and L. Palatinus, *Z. Kristallogr.*, 2014, **229**, 345–352.
22 Z. J. Zhang and X. Y. Chen, *J. Phys. Chem. Solids*, 2009, **70**, 1121–1131.
23 D. R. Kester, I. W. Duedall, D. N. Connors and R. M. Pytkowicz, *Limnol. Oceanogr.*, 1967, **12**, 176–179.
24 *Powder Diffract. File, JCPDS Internat. Centre Diffract. U.S.A.: Data*, 2001, 19073-3273.
25 J. Lu, Q. Han, X. Yang, L. Lu and X. Wang, *Mater. Lett.*, 2007, **61**, 3425–3428.
26 A. Phuruangrat, T. Thongtem and S. Thongtem, *Mater. Lett.*, 2009, **63**, 1496–1498.
27 EPA MINTEQA2 Equilibrium Speciation Model, http://www.epa.gov/exposure-assessment-models/minteqa2, accessed September 2020.
28 I. Langmuir, *J. Am. Chem. Soc.*, 1916, **38**, 2221–2295.
29 H. Freundlich and W. Heller, *J. Am. Chem. Soc.*, 1939, **61**, 2228–2230.
30 B. H. Hameed, *J. Hazard. Mater.*, 2008, **154**, 204–212.
31 F. Homayoon, H. Faghihian and F. Torki, *Environ. Sci. Pollut. Res.*, 2017, **24**, 11764–11778.
32 U. Haseen and A. Hilal, *Ind. Eng. Chem. Res.*, 2020, **59**, 3198–3204.
33 W. Fu and Z. Huang, *Chemosphere*, 2018, **209**, 449–456.
34 R. Sitko, M. Musielak, M. Serda, E. Talik, B. Zawisza, A. Gagor and M. Małecka, *Sep. Purif. Technol.*, 2021, **254**, 117606–117616.
35 M. Li, B. Wang, M. Yang, Q. Li, D. G. Calatayud, S. Zhang, H. Wang, L. Wang and B. Mao, *Sep. Purif. Technol.*, 2020, **239**, 116515.
36 A. S. K. Kumar, S.-J. Jiang and W. L. Tseng, *J. Environ. Chem. Eng.*, 2016, **4**, 2052–2065.
37 Y. Huang, Y. Gong, J. Tang and S. Xia, *J. Hazard. Mater.*, 2019, **366**, 130–139.
38 Y. Yuan, Y. Wu, H. Wang, Y. Tong, X. Sheng, Y. Sun, X. Zhou and Q. Zhou, *J. Hazard. Mater.*, 2020, **386**, 121658.
39 S. Jamshidi, M. K. Rofouei, S. Seidi and Å. Emmer, *Sep. Sci. Technol.*, 2020, **55**, 1505–1514.
40 U. Haseen and H. Ahmad, *Ind. Eng. Chem. Res.*, 2020, **59**, 3198–3204.

41 M. Akbar and M. Manoochehri, *Inorg. Chem. Commun.*, 2019, **103**, 37–42.
42 J. C. García-Mesa, P. Montoro Leal, M. M. López Guerrero and E. I. Vereda Alonso, *Microchem. J.*, 2019, **150**, 104141.
43 M. Shi, X. Yang and W. Zhang, *Anal. Chim. Acta*, 2019, **1074**, 33–42.
44 Z. Es'haghi, G. R. Bardajee and S. Azimi, *Microchem. J.*, 2016, **127**, 170–177.
45 S. Zhang, H. Luo, Y. Zhang, X. Li, J. Liu, Q. Xu and Z. Wang, *Microchem. J.*, 2016, **126**, 25–31.
46 M. Krawczyk and E. Stanisz, *Talanta*, 2016, **161**, 384–391.
47 O. Çaylak, Ş. G. Elçi, A. Höl, A. Akdoğan, Ü. Divrikli and L. Elçi, *Food Chem.*, 2019, **274**, 487–493.
48 S. Seidi and M. Fotouhi, *Anal. Methods*, 2017, **9**, 803–813.
49 H. R. Sobhi, M. Ghambarian, A. Esrafili and M. Behbahani, *Microchim. Acta*, 2017, **184**, 2317–2323.

JAAS

ROYAL SOCIETY OF CHEMISTRY

CORRECTION

View Article Online
View Journal | View Issue

Cite this: *J. Anal. At. Spectrom.*, 2021, **36**, 2017

Correction: Nano-bismuth sulfide based dispersive micro-solid phase extraction combined with energy dispersive X-ray fluorescence spectrometry for determination of mercury ions in waters

Katarzyna Pytlakowska,*[a] Ewa Malicka,[a] Ewa Talik[b] and Anna Gągor[c]

DOI: 10.1039/d1ja90042k

rsc.li/jaas

Correction for 'Nano-bismuth sulfide based dispersive micro-solid phase extraction combined with energy dispersive X-ray fluorescence spectrometry for determination of mercury ions in waters' by Katarzyna Pytlakowska *et al.*, *J. Anal. At. Spectrom.*, 2021, 36, 786–795, DOI: 10.1039/D0JA00477D.

The authors regret an error in the affiliation of one of the authors, Anna Gągor, in the original manuscript. The corrected affiliations for this paper are as shown above.

The Royal Society of Chemistry apologises for these errors and any consequent inconvenience to authors and readers.

[a]*Institute of Chemistry, University of Silesia, Szkolna 9, 40-006 Katowice, Poland. E-mail: katarzyna.pytlakowska@us.edu.pl*
[b]*Institute of Physics, University of Silesia, 75 Pułku Piechoty 1a, 41-500 Chorzów, Poland*
[c]*Institute of Low Temperature and Structure Research, Polish Academy of Science, P.O. Box 1410, 50-950 Wroclaw, Poland*